Development of the X-57 Mod III/IV Piloted Simulator and Discussion of the Resultant Flying Qualities Predictions

Ryan Wallace[1] and James Reynolds[2]
NASA Armstrong Flight Research Center, Edwards, California, 93523, USA

Dana McMinn[3] and David Cox[4]
NASA Langley Research Center, Hampton, Virginia, 23681, USA

The all-electric X-57 Mod III aircraft was designed to demonstrate wingtip propulsion drag reduction benefits on a high-aspect-ratio wing. The X-57 Mod IV aircraft was designed to expand on the Mod III version and demonstrate the benefits of distributed electric propulsion. This paper discusses the development of the all-electric X-57 Mod III and Mod IV fixed-base pilot-in-the-loop nonlinear simulator. The paper describes the model development and the simulator cockpit construction for uses such as flight training and flying qualities analysis. Results from a stability and flying qualities analysis for both Mod III and Mod IV are presented. These results predict that both Mod III and Mod IV are stable throughout their flight envelopes. Mod III is predicted to have satisfactory flying qualities while Mod IV is predicted to have areas of adequate flying qualities.

I. Nomenclature

C_D	=	drag coefficient
C_L	=	lift coefficient
C_M	=	pitching moment coefficient
Fs	=	stick force
g	=	gravity
H_{MSL}	=	altitude (mean sea level)
Kpo	=	overspeed protection gain
Kpu	=	underspeed protection gain
n/α	=	load factor as a function of angle of attack
p	=	roll rate
q	=	pitch rate
r	=	yaw rate
$Stick_F$	=	stick feel feedback force
$Torq_{Cmd}$	=	commanded torque lever position
$T_{increase}$	=	amount of torque added
$Torq_{out}$	=	motor-generated torque
T_{reduce}	=	amount of torque reduced
u	=	longitudinal velocity in the body axis
V_t	=	true airspeed

[1] Aerospace Engineer, Flight Dynamics and Control Branch, AIAA Senior Member.
[2] Aerospace Engineer, Flight Dynamics and Control Branch, nonmember.
[3] Aerospace Engineer, Dynamic Systems and Control Branch, AIAA Member.
[4] Aerospace Engineer, Dynamic Systems and Control Branch, AIAA Senior Member.

v = lateral velocity in the body axis
w = vertical velocity in the body axis
α = angle of attack
β = sideslip angle
Δ = difference between two values of the same term
δa = aileron deflection
δe = elevator deflection
δr = rudder deflection
ζ = damping ratio
ζ_{DR} = Dutch roll damping ratio
ζ_{Ph} = phugoid damping ratio
ζ_{SP} = short-period damping ratio
τ_r = roll mode time constant
Φ = roll angle
Ω = motor speed
$\Omega high$ = upper motor speed limit
Ωlow = lower motor speed limit
ω = frequency
ω_{SP} = short-period frequency

II. Introduction

The National Aeronautics and Space Administration (NASA) X-57 "Maxwell" project was purposed to investigate the potential benefits of distributed electric propulsion (DEP) on a general aviation aircraft and the potential reduction of drag utilizing wingtip propulsion. To reduce developmental risk, the project had three phases, each numbered consecutively and termed a "Mod" (for "modification"). Each successive Mod was to add capability to the aircraft, as shown in Fig. 1.

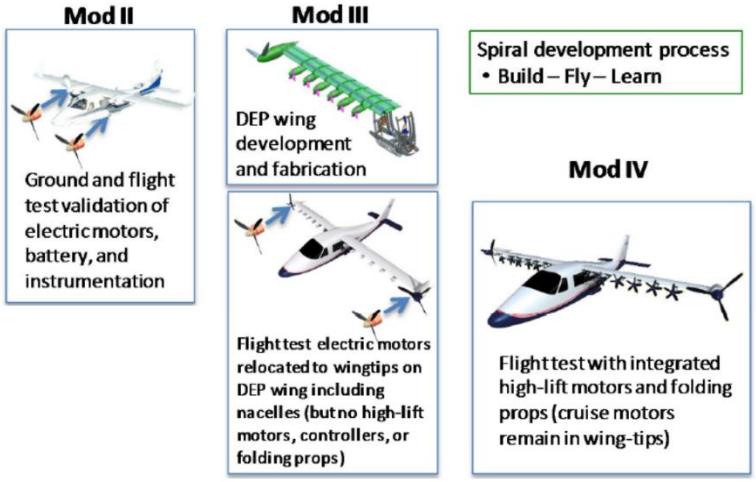

Fig. 1 Overview of the X-57 Maxwell project [2].

A Tecnam (Costruzioni Aeronautiche Tecnam srl) (Capua, Italy) P2006T twin engine aircraft was purchased by the X-57 project team to be used as the base platform to be modified into an electric aircraft. The modification, termed Mod II, replaced the existing P2006T gasoline-powered engines with JM-57 electric cruise motors constructed by Joby Aviation, Inc. (Santa Cruz, California). Two main batteries with 23 kWh of usable capacity were developed by Electric Power Systems Inc. (Industry, California) to power the cruise motors. These batteries were installed along with the supporting electrical system as described in Clarke et al.[1] and shown in Fig. 2. The change from gasoline-powered engines to electric motors required the power pilot inceptors also to be replaced. The X-57 project test pilot commands the cruise motor power by commanding a torque level and a motor speed. Mod III would utilize the same electrical system as Mod II while Mod IV would be expanded to incorporate the distributed electric propulsion system (also known as the high-lift system), also shown in Fig. 2.

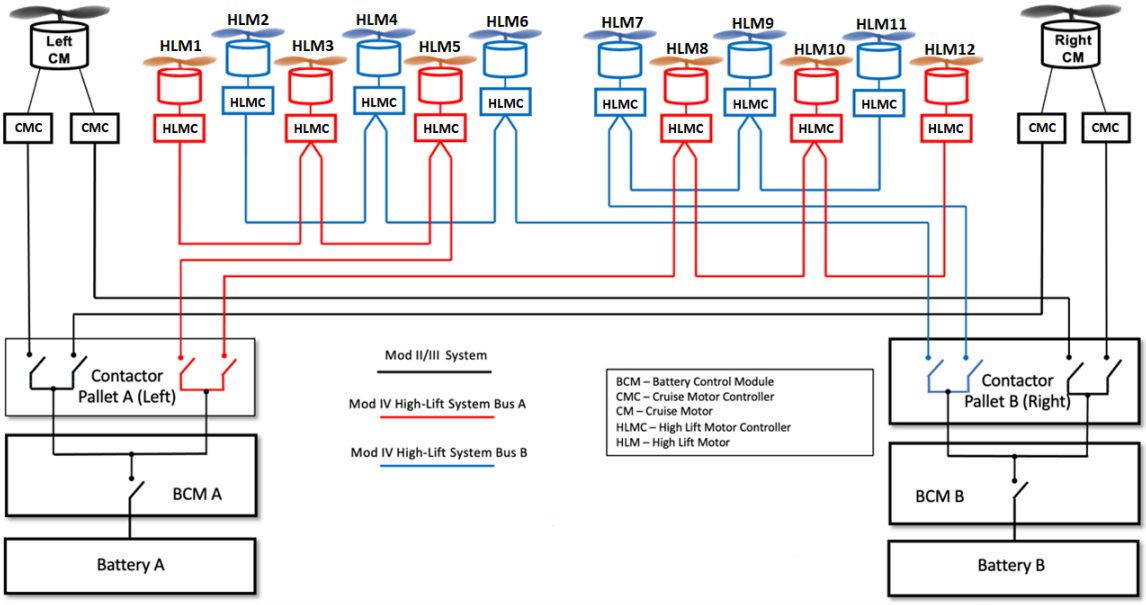

Fig. 2 Electric propulsion systems: Mod II, Mod III, and Mod IV.

The Mod III phase would reduce the drag of the aircraft by replacing the P2006T wing with a cruise-optimized wing having an aspect ratio of 15.0, a span of 31.6 ft, and a wing loading of 45.0 lbf/ft2. As described in Borer et al. [2] the wing was optimized for reducing drag during the cruise phase of flight. The Mod II cruise motors would be repurposed for Mod III and relocated onto the wingtips of the cruise-optimized wing to reduce drag from the wingtip vortices. Dummy nacelles were added along the wing where the high-lift motors would be placed in Mod IV. Due to the replacement of the wing, the landing configuration stall speed is 73 knots calibrated airspeed (KCAS), the takeoff configuration stall speed is 80 KCAS, the reference airspeed is 94 KCAS, and the minimum control speed is 85 KCAS. The aircraft would be capable of reaching 14,000 ft MSL; the X-57 project had an operational ceiling of 10,000 ft MSL.

Finally, Mod IV would add a high-lift system consisting of 12 additional electric motors with fixed-pitch propellers along the leading edge of the Mod III cruise-optimized wing. The high-lift system would generate blown lift over the wing at low speeds where the Mod III wing is not optimized for producing lift. When not powered on, the high-lift system propeller blades were designed to fold lengthwise along the nacelles to reduce drag. With the high-lift system activated, the landing configuration stall speed is 58 KCAS, the takeoff configuration stall speed is 70 KCAS, the reference airspeed is 75 KCAS, and the minimum control speed is 84 KCAS. The high-lift system was intended to be operated only while the aircraft is either in takeoff or landing configurations. The Mod IV would have the same operational ceiling as Mod III (10,000 ft MSL).

Some of the aircraft systems will not be modified. The surface control system will remain a cable-and-pulley reversable system. The landing gear and associated mechanisms will not be modified. The fuselage will only be modified to mount the batteries and new wing.

This paper focuses on the development of a pilot-in-the-loop simulator for the Mod III aircraft and the Mod IV aircraft. A brief description of the simulator models and how they were developed is given, along with description of the simulator cockpit. This paper also discusses the stability analysis conducted on the Mod III and the Mod IV aircraft, and presents a flying qualities assessment of both aircraft throughout their expected flight envelopes.

III. Piloted Simulator Development

The X-57 project team developed both a desktop and a pilot-in-the-loop simulator to provide a method to predict the stability and flying qualities of the X-57 Mod III and Mod IV aircraft. In addition to flying and handling qualities assessments, the pilot-in-the-loop simulator provided a platform for developing emergency scenario training and flight maneuver development.

A. Simulator Architecture

The simulator integration flow chart is given in Fig. 3.

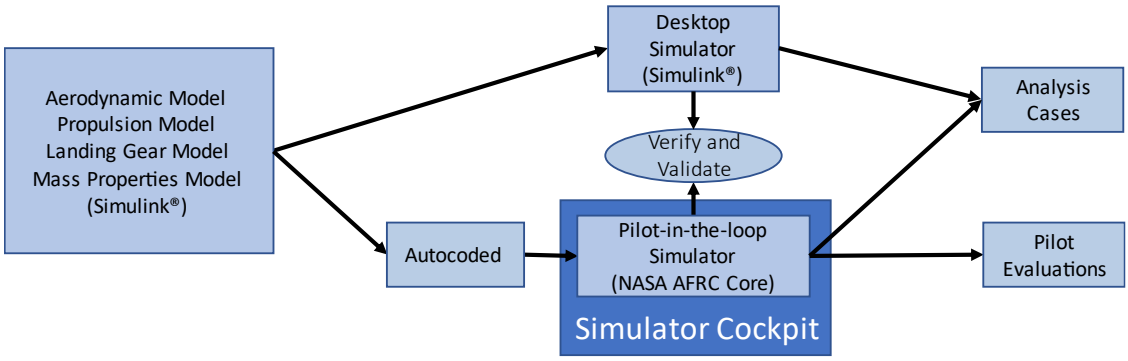

Fig. 3 Flowchart of the X-57 simulator integration.

Vehicle models of the aerodynamics, propulsion, landing gear, and mass properties were developed in by the X-57 project team to represent the vehicle environment and hardware. The vehicle models, described below, were generated using the commercial software, MATLAB® R2016b and Simulink® R2016b (both of The MathWorks, Inc., Natick, Massachusetts) [3]. A desktop simulator was then constructed through integration of the vehicle models in a Simulink® simulation environment. All of the models and the desktop simulator ran at 200 Hz.

Building upon the desktop simulator, a fixed-base pilot-in-the-loop simulator cockpit was constructed and driven by integrated autocoded C++ versions of the Simulink® models into the NASA Armstrong Flight Research Center (AFRC) (Edwards, California) Core Version 7 simulation architecture software [4]. The models were individually autocoded and then integrated into the Core simulation software. The pilot-in-the-loop simulator software also ran at 200 Hz.

The integration of the pilot-in-the-loop simulator models was validated by comparing simulation data from the pilot-in-the-loop simulator to that of the desktop simulator. The simulations cases used for validation were run in both simulators to highlight the aerodynamic, propulsion, and landing gear model data outputs at multiple flight conditions and in various locations in the flight envelope. The desktop simulator data were taken as the truth source. An example of a desktop simulator (Sim) to a pilot-in-the-loop (PIL) simulator validation test can be seen in Fig. 4. Figure 4 shows a comparison between the data from a simulation flight conducted by one of the X-57 project test pilots in the pilot-in-the-loop simulator and the data from a desktop simulation with the same flight conditions and control inputs as the pilot-in-the-loop simulation. The data from both simulations match.

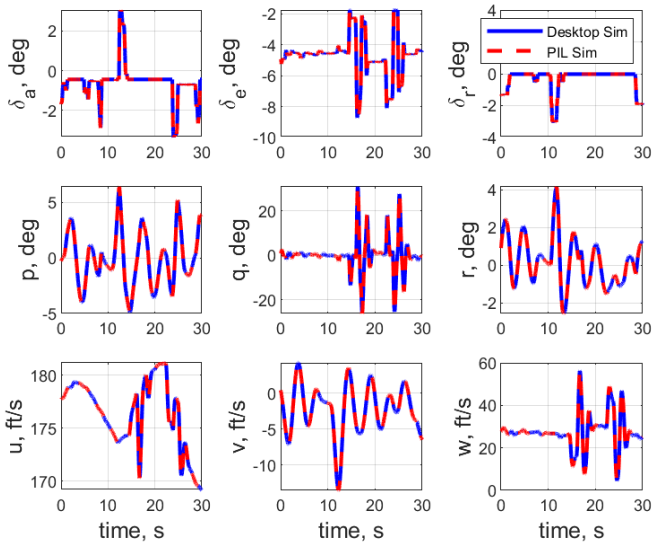

Fig. 4 Example of validation of the pilot-in-the-loop simulator to the desktop simulator.

The X-57 project test pilots performed independent verification of the pilot-in-the-loop simulator cockpit hardware by testing the hardware functions. This testing included verifying that each pilot inceptor, gauge, and switch on the simulator cockpit would work in the same way as would the hardware on the aircraft.

B. Simulator Model Development

The Mod III and Mod IV models were developed by various discipline teams within the X-57 project teams for the desktop simulator and pilot-in-the-loop simulators. The models described here include the propulsion model, aerodynamic model, landing gear model, and the mass properties model.

1. Propulsion Model

The overall propulsion model is composed of subsystem models of the high-lift motors, cruise motors, and battery. The propulsion model provided the forces and moments from the cruise motors and the high-lift system. In addition to the forces and moments, the model also outputs the voltage, current, and power of the batteries and motors.

The cruise motor (CM) and cruise motor controller (CMC) are modeled like those of the Mod II simulator electric motor system as described in Wallace et. al. [5]. The two CMs are modeled as a proportional torque input to motor shaft power output system. Like the aircraft power system, the propulsion model has two CMCs suppling power to a single cruise motor. Efficiency losses for both the CMs and the CMCs are accounted for in the propulsion model. Efficiency values from a lookup table are applied to the current draw of the CMs while a constant, nominal efficiency of 97 percent is applied to the current to represent the current losses in the CMCs.

The CMCs in the model utilize the aircraft mapping of the CM torque inceptor position to motor torque command. The mapping has three major operational regions: regeneration, nominal, and overdrive. The regeneration region, -17.4- to -0.7-percent lever position, commands a negative torque to the CM that drives the propellers to windmill, which increases the drag torque on the CM. The nominal region, -0.7- to 100-percent lever position, commands a positive torque to the CM. The CMCs were designed to produce 127.5 Nm of CM torque when at 100 percent torque command and 2700 rpm. Idle command is between the -0.7- to 6.5-percent lever position, where the CMs produce little to no thrust but still are rotating. For additional thrust, the overdrive region, above the 100-percent lever position, has the capability of producing 175 Nm of torque per CM. The overdrive region was designed for use with only one operational CMC per CM.

In addition to supplying power to the CMs, the CMCs in the propulsion model provide overspeed and underspeed protections to the CMs. The CMCs apply conditional torque weights, represented by Eq. (1) and Eq. (2):

$$T_{reduce} = K_{po}\left(\Omega - \Omega_{high}\right)^2 \tag{1}$$

$$T_{increase} = K_{pu}(\Omega - \Omega_{\text{low}})^2 \quad (2)$$

where K_{po} is the overspeed protection gain, K_{pu} is the underspeed protection gain, (Ω - Ω_{high}) is the difference between the CM speed and the upper speed limit, and (Ω-Ω_{low}) is the difference between the CM speed and the lower speed limit. The CM speed protection was designed to activate the overspeed protection when the CM speed is above 2750 rpm; the underspeed protection activates when the CM speed is below 1100 rpm.

The constant-speed propeller system for the CMs in the propulsion model is based on the Electric Variable Pitch Propeller (MT-Propeller USA, Inc., DeLand, Florida) [6] used on the aircraft. In the propulsion model the CM propeller hubs adjust the pitch angle of the blades based on the commanded rpm and airspeed in a rate limited servo loop system. Blade Element Momentum (BEM) predictions obtained by the open-source software, XROTOR [7], provided the CM propeller advance ratios, thrust coefficients and torque coefficient. The advance ratio and torque predictions were also used in a computational fluid dynamics (CFD) analysis for the aerodynamic model. Propeller and motor inertial responses to torque and inertial coupling due to vehicle rates are modeled.

For the high-lift system, the model included 12 motors with fixed-pitch propellers that folded back when not active as described by Patterson, Borer, and German [8]. The high-lift motors had two operating modes between which the X-57 project test pilot could select: airspeed control and fixed-speed control. In airspeed control mode the motor speed was scheduled based on airspeed and altitude to optimize the lift over the wing generated by the motors based on BEM analysis [9]. Wind-tunnel testing of the high-lift propellers allowed for further refinement of the high-lift motor torque output based on rpm [10]. The operational range was from 58 KCAS to 90 KCAS; above 90 KCAS the motors still operate but the motor speed becomes non-optimized for generating lift. The fixed-speed control mode sets the motor speed to 4800 rpm to optimize the amount of thrust versus motor performance. Figure 5 shows the high-lift (HL) system motor speeds at 6000 ft for a range of airspeeds in both airspeed and fixed-speed mode. The spin direction for the high-lift motors alternated such that each pair of motors was counter-rotating.

In the propulsion model, the high-lift motors were grouped in sets of three, based on the grouping of the contactor pallet shown in Fig. 2. Contactor pallet A powers the set of high-lift motors #1, #3, and #5 as well as the set of motors # 8, #10, and #12. Contactor pallet B powers the set of high-lift motors #2, #4, and #6 as well as the set of motors # 7, #9, and #11. Failures of the high-lift motors happen in the described sets of three.

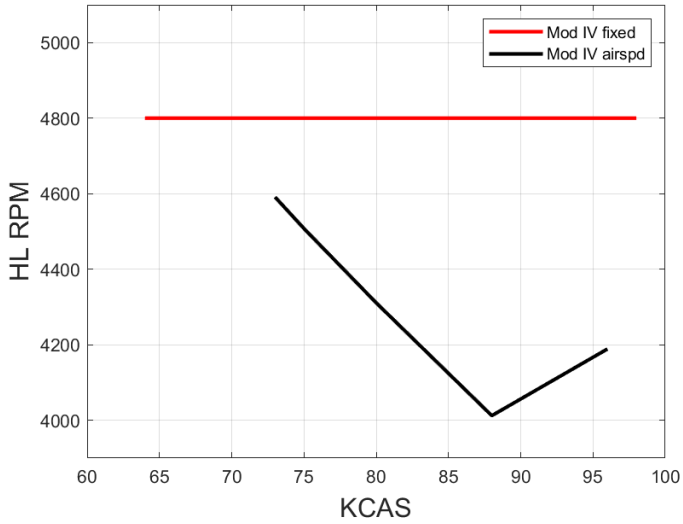

Fig. 5 Mod IV high-lift motor rpm versus airspeed at 6000 ft.

The battery model, described in detail in Chin et al. [11], is a Thevenin Equivalent Circuit Model based on the X-57 battery system. The battery model uses the current draw to the motors to estimate battery voltage, power, temperature, and state of charge. The battery model also takes into account the operational state of the CMCs, that is, if a CMC is switched off the battery model will take that change into account in the power draw.

A key feature within the simulator for pilot emergency training is a set of propulsion system failures. Generated within the propulsion model, the possible failures include cruise motor power failures, propeller hub failures, high-lift motor power failures, and power command failures. The CMC power failures could fail two of the four CMCs

individually or simultaneously. The cruise motor failures and the propeller hub failures could be triggered for left, right, or both. High-lift system failures include full power failure for three high-lift motors on one side, three high-lift motors on both sides, six high-lift motors on one side, or all high-lift motors. Command power failures could fail the command to the left, right, or both motors. Different failure types cannot be triggered simultaneously; for example, a high-lift system failure cannot be triggered at the same time as a propeller hub failure. Table 1 lists the available simulator propulsion failures.

Table 1 Available simulator propulsion system failures: Mod III and Mod IV.

Failure Type	Failure Description
Fail Cruise Motor Controller	Half power failure to cruise motor, half the motor thrust produced.
Full cruise motor failure, propeller forces remain	Full power failure to cruise motor, no thrust produced. Propeller forces remain.
Full cruise motor failure, no propeller forces	Full power failure to cruise motor, no thrust produced. No propeller forces remain.
Fixed-pitch propeller failure	Propeller blade pitch fixed in position.
Fail motor to half power and freeze propeller hub	Half power failure to cruise motor, half the motor thrust produced. Propeller bland pitch angle fixed.
Fail motor to zero power and freeze propeller hub	Full power failure to cruise motor, half the motor thrust produced. Propeller bland pitch angle fixed.
Feathered propeller instantaneous failure	Propeller blade pitch instantaneously goes to feather position
Motor command failure, 1 cruise motor	Torque command to single cruise motors fixed.
Motor command failure, 2 cruise motors	Torque command to both cruise motors fixed.
Runaway hub toward max pitch (feather)	Propeller blade pitch move to feather position.
Runaway hub toward min pitch (windmill)	Propeller blade pitch move to windmilling position.
3 High-lift motors, same wing failure (Mod IV only)	Full power failure to 3 high-lift motors on one side.
6 High-lift motors, same wing failure (Mod IV only)	Full power failure of 6 high-lift motors on one side.

Each of the failures was examined by the X-57 project test pilots in the pilot-in-the-loop simulator. Although failure analysis is outside the scope of this paper, work done by Wallace et al. shows the impact of a cruise motor failure in the Mod III configuration [12]. This work showed that an abrupt full cruise motor failure during takeoff and climbout represents a potentially catastrophic event.

2. Aerodynamic Model

Extensive development has gone into the Mod III/IV aerodynamic model [13-16]. Four different CFD solvers were used in the development of the aerodynamic database: StarCCM+ (Siemens, Munich Germany) code [17]; Launch, Ascent, and Vehicle Aerodynamics (LAVA) code [18]; USM3D code [19]; and KESTREL code [20]. All cases were run as fully turbulent using the Spallart-Allmaras turbulence model [21].

The full aerodynamic model is an amalgamation of the power-off aerodynamics, cruise motor effects, high-lift motor system effects, and a set of propulsion failures. The model also includes ground effects and aerodynamic uncertainties. The power-off aerodynamics represent the baseline case in which the cruise motor, high-lift motor system, and failure aerodynamic effects are added onto as flight conditions require. These added aerodynamic effects are added to baseline case through coefficient deltas, as defined in Eq. (3).

$$\Delta C = C_{power\ on} - C_{power\ off} \tag{3}$$

The paper by Fredrick et al. [16] provides a detailed description of the aerodynamic coefficient results from the CFD analysis.

The initial CFD cases, termed the "power-off cases," provided a model of the Mod III/IV airframe with no cruise motor or high-lift propulsor effects [14]. These cases investigated sweep of angles of attack (α) from -2 to 22 deg as well as sideslip angles (β) from 0 to 20 deg for neutral control surface positioning and three flap deflections: 0 deg, 10 deg, and 30 deg. The CFD analysis provided lift coefficient, drag coefficient, pitching moment coefficient, side force coefficient, rolling moment coefficient, and yawing moment coefficient as functions of α, β, and flap deflections. Additional power-off CFD analysis was performed to determine the forces and moments generated by the control surfaces. The full range of elevator, rudder, and aileron deflections were examined individually for 2 deg, 8 deg, and predicted stall angles of attack for each flap deflection position.

The cruise motors aerodynamic effects on the aircraft were predicted by a set of CFD cases at various freestream speeds to the blade tip speed ratios (called advanced ratios) and blade pitch angles. The advanced ratios, thrust outputs and blade pitch angles were from the propulsion model BEM results. The cruise motor CFD study examined a sweep of advance ratio values from 0.4 to 1.8 at set blade pitch angles from 14 to 40 deg. This range of advance ratios and blade pitch angles represents the expected power-on flight envelope of the aircraft. From the CFD study, the cruise motor power-on deltas (ΔC_D, ΔC_L, and ΔC_M) were modeled as function of advance ratio and blade pitch angle.

Similar to the cruise motor aerodynamic case study, a large set of CFD runs was conducted using the advance ratios results from the high-lift motor BEM propulsion model to predict the aerodynamic effects of the high-lift system upon the aircraft. The CFD cases were examined at airspeeds from 35 KCAS to 110 KCAS, with flap settings of 10 deg and 30 deg down. For high-lift system failures, this aerodynamic data set also included various combinations of active and inactive high-lift motors. From the CFD study, the high-lift motor power-on deltas (ΔC_D, ΔC_L, and ΔC_M) were modeled as function of advance ratio. Detailed results of the high-lift system CFD studies can be found in Ref. 15.

The landing gear for the Mod III and Mod IV aircraft would have been the same as the landing gear for the Mod II aircraft, so the landing gear aerodynamic effects were common to all Mods. The landing gear drag and pitching moment increments were derived from parameter identification analysis on a Tecnam P2006T flown at AFRC in 2014 [5].

The hinge moments for the aileron and elevator control inceptor were contained in the aerodynamic model. The model utilized the predicted forces generated by the control surfaces as well as the equivalent moment arms from the inceptor to the control surfaces to calculate the hinge moment.

Ground effects were included in the aerodynamics model from 5.8 ft to 31.2 ft above ground level. The model was developed using CFD analysis with a moving wall ground plate. Following best practices two solvers were used: the STAR-CCM+ solver with a viscous wall, and the LAVA solver with an inviscid wall. In both the takeoff configuration and in the landing configuration, an angle-of-attack sweep was performed with no power, only cruise motor power, and only high-lift system power. The analysis provided a delta for ΔC_L and ΔC_M based on motor power, angle of attack, and height above the ground.

Uncertainty parameters were included for the aerodynamic coefficients and rate derivatives within the aerodynamic model to account for uncertainty. The power-off aerodynamic and the control surface uncertainty parameters were an additive value onto the coefficients, while the cruise motor and high-lift system uncertainty parameters were a multiplicative value. Further details of the uncertainty parameter development can be found in Fredrick et al. [16].

3. Landing Gear

The landing gear model for the Mod III and the Mod IV aircraft was the same as for the Mod II aircraft, described in further detail in Wallace et al. [5]. The nose gear was modeled as a linear compression spring-damper post. The main gear was modeled as trailing arms with a spring-damper system. Each tire was modeled with compressibility effects.

4. Mass

A high-fidelity computer-aided design (CAD) model was generated for the Mod III and the Mod IV aircraft with the dimensions and weights of the individual aircraft components and subsystems. This CAD model allowed for tracking of the aircraft mass properties of the overall weight of aircraft, moments of inertia, and center of gravity (CG). The aircraft mass properties were then integrated into the simulation mass model. The aircraft were projected to have an overall weight of 3075 lb. The moments of inertias (Ixx, Iyy, Izz) were projected to be 18.6812e6, 8.35934e6, and 25.2127e6 lb/in2, respectively; and the cross-product moments of inertias (Ixy, Ixz, Iyz) were projected to be 1.5528e3, 3.213e4, and 3.7987e2 lb-in2, respectively. Based on the component weights and placements, the aircraft had a projected longitudinal CG of 28.6 percent of the mean aerodynamic chord, lateral CG of 1.19 in to the left of the aircraft centerline, and a vertical CG of 21.2 in below the leading edge of the wing.

C. Simulator Cockpit

To have a realistic-as-possible pilot-in-the-loop simulator the simulator cockpit was designed to be similar to the Mod III and the Mod IV aircraft. Figure 6 shows the fixed-base pilot-in-the-loop simulator at AFRC. The Mod III simulator and the Mod IV simulator used the same hardware as did the Mod II simulator described in Wallace et al. [5]. Additional switches and indicator lights were added to the simulator cockpit for the Mod IV configuration to operate the high-lift system.

Fig. 6 The X-57 fixed-base pilot-in-the-loop simulator.

The cockpit consists, as seen in Fig. 7, of a dashboard, yoke, rudder pedals with toe brakes (not shown), cruise motor control inceptors, overhead motor power switch panel, and a pilot seat. The dashboard consists of a heads down display (HDD), multifunction display (MFD), and aircraft non-propulsion system switches.

Fig. 7 The X-57 pilot-in-the-loop simulator cockpit dashboard, control surface inceptors, motor power control inceptors, and overhead switch panel.

The HDD for Mod IV is shown in Fig. 8. The right and the left panel of the HDD utilized two touch-screen monitors to display the instrumentation gauges as well as articulating the high-lift system. By using touch-screen monitors, X-57-specific digitally displayed gauges and switches could be quickly updated to match what would be installed in the aircraft as the project team updated instrumentation and switches throughout the development cycle. Thus, the touch-screen monitors eliminated the need to purchase and integrate aircraft hardware into the simulator. Digitally displayed gauges and switches also allowed the X-57 project test pilots to review the purposed hardware appearance and behavior before installation in the aircraft. The white shaded box in Fig. 8 displays the high-lift system arm switch, high-lift system operational mode switch, and six LED high-lift system status indicators. The orange

shaded box in Fig. 8 displays the annunciator panel in which a yellow or a red box illuminates when there is either a caution or warning, respectively, due to a system failure. The green shaded box in Fig. 8 displays the voltage, current, and power being supplied from the cruise motors controllers to the motors. The red shaded box in Fig. 8 displays the avionics voltage and current draw from the electric system. The other shaded boxes in Fig. 8 display the radio (top purple), accelerometer (bottom purple), flap indicator (brown), and motor tachometers (blue).

Fig. 8 The X-57 piloted simulator heads down display (HDD): (left) panel includes stock P2006T instruments (no shading); annunciator panel (orange shading); high-lift system control switches (white shading); radio (top purple shading); and accelerometer (G-meter) (bottom purple shading); and (right) panel includes tachometers (blue shading); avionics power meters (red shading); flap indicator (brown shading); and battery power meters (green shading).

Situational awareness of the state of the aircraft is critical to a pilot's ability to take appropriate action in the case of a failure or emergency condition. Multiple aural alerts in the form of audio messages were provided in the simulator. These audio messages include cautions and warnings for avionics power out of limits, battery failures, low voltage, motor controller failures, propeller overspeed, and propeller controller failures. In addition to aural alerts the X-57 project test pilot was provided with illuminated alerts on the annunciator panel, located on the left-hand panel of the HDD (orange shaded box in Fig. 8).

Three sets of lights in the middle of the dashboard displayed cruise propeller information to the X-57 project test pilot. These lights can be seen in the white shaded box in Fig. 9. A set of blue lights indicates when the propeller blade angle is being driven toward feather (high blade pitch angle), a set of green lights indicates when the propeller blade angle is in the start position (low blade pitch angle), and a set of yellow lights indicates that there is a propeller hub system internal fault. The left-hand lights correspond to the left cruise propeller and the right-hand lights correspond to the right cruise propeller.

The MFD, seen in the yellow shaded box of Fig. 9, is a controller area network (CAN) bus reader located on the center of the dashboard that provided real-time information. Information presented to the X-57 project test pilot included the state of the main batteries, propulsion system power, and propulsion system temperatures. A detailed description of the MFD and the associated CAN bus messaging system for the X-57 aircraft can be found in Clarke, Curry, and Samuel [22]. The MFD system includes a page selector knob and a fault page switch, also shown in the shaded yellow box of Fig. 9.

Fig. 9 The X-57 pilot-in-the-loop simulator multifunction display (yellow shaded box) and propeller indicator lights (white box).

The stock angle-of-attack probe was located on the stock wing, which was replaced with a cruise-optimized wing, so neither the Mod III aircraft and nor the Mod IV aircraft has a stall warning system available. The X-57 project test pilot thus was restricted to airspeeds well above predicted stall speed in order to avoid stall during flight.

Identical switches were installed into the simulator cockpit at the same locations to ensure that the X-57 project test pilots developed familiarization of the location and operation of critical switches within the aircraft cockpit. Each switch in the simulator has the same part number as its counterpart on the aircraft to ensure the same action and feel. The switches for the essential bus, DC converters, cross buses, wing avionics, and avionics buses are located on the dashboard. Also located on the dashboard, below the HDD right-hand panel, are the propeller pitch controller switches, which control the operational mode of the propeller hub and the manual setting of the propeller pitch angle. The switches for activation of the cruise motors are located on an overhead panel in both the aircraft cockpit and the simulator cockpit. The switches are locking type, in order to prevent accidental disarmament of a power switch.

The control surface inceptors of the X-57 aircraft were replicated in the simulator cockpit to provide the X-57 project test pilots with a positive training feel for controlling the aircraft. The X-57 right-hand yoke would not be used during flight; therefore, that yoke was repurposed for the simulator cockpit, providing additional feel familiarity. The yoke controlled the ailerons and elevators and was connected to a force feedback feel system. The force feedback system provided the X-57 project test pilots with predicted forces generated by the ailerons and elevator hinge moments from the aerodynamic model. The X-57 project test pilots based their assessment of the force feedback for Mod III and Mod IV on their experience with the Mod II and the P2006T aircraft. The rudder and nosewheel steering were controlled by a rudder pedal assembly which included toe brakes. The toe brakes, one on each rudder pedal, provided differential braking. Flap position was controlled by a flap switch located on the dashboard.

Commanding the cruise motors in the simulator, as in the X-57 aircraft, was achieved by two torque-input levers and two propellor pitch levers - one for each cruise motor. The torque-input levers provide torque-input signals to the motor controllers that provided the requested power to drive the cruise motors. Lever detents separated the three distinct torque-input regions to prevent accidental pilot command. For cruise motor rpm control, a desired rpm was commanded using the propeller pitch levers, which drive the propeller pitch angle to achieve the desired cruise motor speed. At the full aft propeller pitch lever position a switch could command the propeller pitch angle to maximum.

In Mod IV simulated landings with the high-lift system active, the X-57 project test pilots found that after touching down the brakes were ineffective for stopping the aircraft rollout. A method was needed to eliminate the residual thrust being produced by the high-lift system. A high-lift system disarm button was integrated on the yoke to quickly de-energization the high-lift system. This button, pictured in Fig. 10, also provided a quick way to disarm the high-lift system in case of a high-lift system failure during flight.

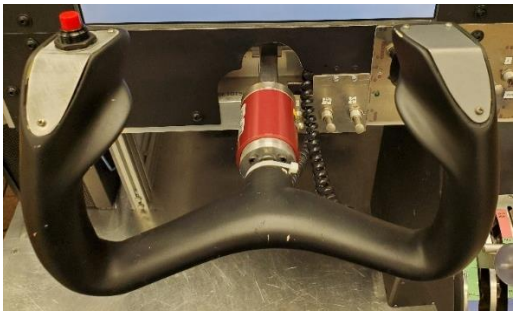

Fig. 10 The X-57 pilot-in-the-loop simulator yoke with high-lift disarm button (red button).

Realistic out-the-window visuals were created by three projectors onto a curved 120 horizontal deg by 34 vertical deg field-of-view screen. The projection scenes merged by way of an optical blender that ensures a continuous out-the-window field-of-view. The system had a time delay of 70 ms from pilot input to screen output.

The simulator cockpit also includes the right seat for the X-57 aircraft.

D. The X-57 Project Test Pilots

The X-57 project employed two NASA test pilots to conduct the pilot-in-the-loop simulations. Both pilots are graduates of the United States Air Force Test Pilot School and each has decades of experience flying experimental aircraft.

IV. Flying Qualities of the Mod III and the Mod IV Aircraft

Although this paper cannot contain an exhaustive assessment of airworthiness, the Mod III and the Mod IV aircraft piloted simulator was utilized to help predict the flying qualities of both aircraft. The airworthiness prediction discussion within this paper is an assessment of the static and dynamic stability at various points throughout the potential flight envelopes. For Mod III, the cruise configuration, takeoff configuration, and landing configurations are examined; for Mod IV only the takeoff and landing configurations are examined. The flaps and gear were retracted for the cruise configuration; the flaps were set to 12 deg and landing gear deployed for the takeoff configuration; the flaps were set to 30 deg (full deployment) and landing gear deployed for the landing configuration. For purposes of clarity, most of the figures presented below show the results from the takeoff (TO) configuration; the other configurations show trends similar to those of the takeoff configuration for both Mod III and Mod IV.

A. Stability Analysis

The X-57 project team utilized Federal Aviation Regulations (FAR) Part 23 to provide guidance for longitudinal and lateral static stability predictions through pilot-in-the-loop simulations [23]. Pilot-in-the-loop simulations were conducted to predict longitudinal static stability utilizing FAR §23.173 and the corresponding FAR §23.175. Piloted simulations were conducted employing FAR §23.177 for lateral static stability guidance. Stability predictions were also made using batch simulations by examining the aerodynamic coefficients and control surface position at various points in the flight envelope.

The FAR §23.173 requires that the control system friction is not excessive and that the stick force curve versus airspeed is sufficiently steep for safe operations. The FAR §23.175 expands on FAR §23.173 by describing the procedure used to determine the stick force curve based on pilot opinion and aircraft ability to stick-free return-to-trim conditions. The requirements were demonstrated for both the Mod III and the Mod IV aircraft in the pilot-in-the-loop simulator through two independent maneuvers. The maneuvers were conducted at various aircraft flap configurations, altitudes, and airspeeds to ensure stability throughout the flight envelope. The pilot-in-the-loop maneuvers for the Mod IV aircraft were conducted in airspeed mode.

The first maneuver had the pilot trim the aircraft to zero out the yoke forces. The pilot then held a longitudinal yoke displacement to capture 10 KCAS off-trim speed. The pilot would note the yoke force direction and amplitude required to maintain the off-trim speed. Both the Mod III aircraft and the Mod IV aircraft (in airspeed mode) showed positive speed stability, as seen in Fig. 11. A push of the yoke sees a predictable increase in airspeed and a positive stick restoring force for the Mod II aircraft; a push of the yoke sees, as expected, an increase in airspeed for the Mod IV aircraft. The Mod IV fixed mode had similar response to that of Mod III, therefore was not included in Fig. 11.

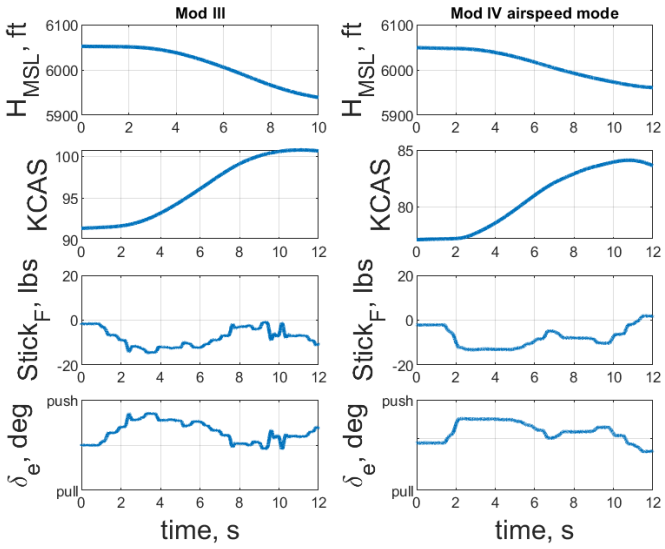

Fig. 11 Simulator time history of a longitudinal yoke displacement for the Mod III aircraft and the Mod IV aircraft in takeoff configuration.

The second longitudinal maneuver, again beginning in trim, had the pilots apply a longitudinal yoke displacement, then slowly release the yoke, and observe if the aircraft would return to within ±10 percent of the initial trim speed. Figure 12 shows the piloted simulation data of the maneuver results for the Mod III aircraft for the takeoff configuration (left panels) and the cruise configuration (right panels). Figure 13 shows the piloted simulation data of the maneuver results for the Mod IV aircraft with the high-lift system in fixed mode (left panels) and in airspeed mode (right panels). A pull of the yoke for the Mod III aircraft shows a stable stick-free return to within the ±10 percent of the initial trim speed. The Mod IV aircraft also shows a stable stick-free return to within the ±10 percent of the initial trim speed for a push of the yoke. Comparing both figures, the number of oscillations to return to trim speed between the Mod III aircraft and the Mod IV aircraft indicates that the high-lift system is having an effect on the longitudinal damping. The bottom right panel of Fig. 13 shows that the high-lift system is responding to the perturbation in airspeed, which might be increasing the damping when compared to the fixed-mode case.

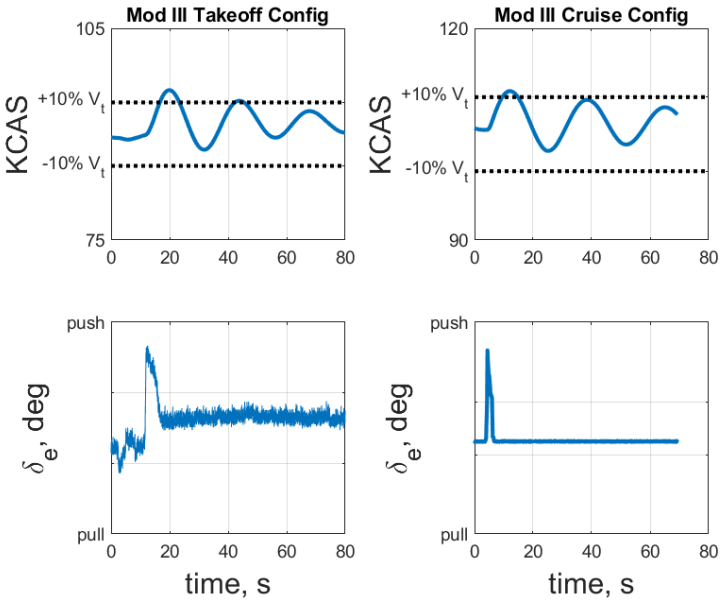

Fig.12 Simulator time history of a longitudinal yoke perturbation for the Mod III aircraft.

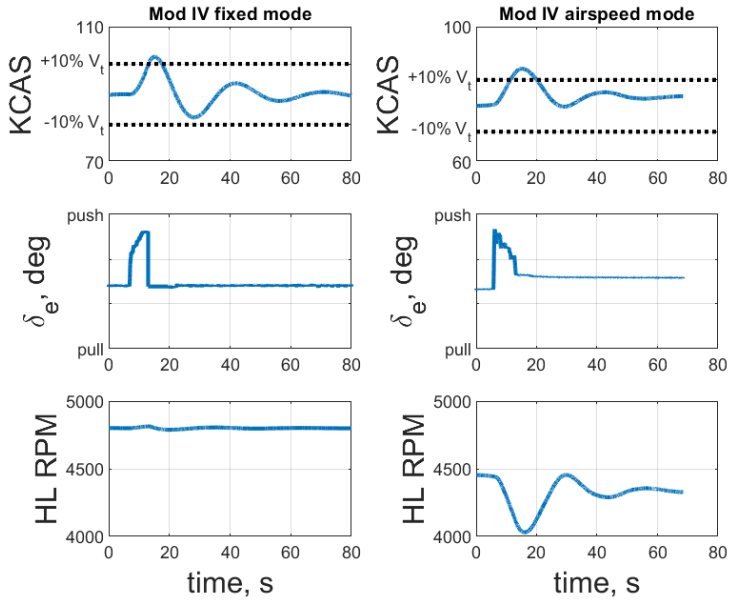

Fig. 13 Piloted simulator time history of a longitudinal yoke perturbation for the Mod IV aircraft in takeoff configuration: high-lift system in fixed mode (left) and in airspeed mode (right).

A classic method of determining the longitudinal stability of the aircraft was conducted through simulation analysis by examining the pitching moment coefficient (C_M) versus the angle of attack (α). The aircraft is longitudinally statically stable if the slope of the C_M versus angle-of-attack curve is negative [24]. In Fig. 14 both the Mod III aircraft and the Mod IV aircraft show a negative slope for the C_M versus angle-of-attack curve. There is a clear shift up in the Mod IV aircraft of the C_M for the same angles of attack when the high-lift system is in airspeed mode. The high-lift system in fixed-speed mode only shifts the C_M for higher angles of attack when in the landing configuration, indicating that the increased lift over the wings for the high-lift system is also altering the C_M.

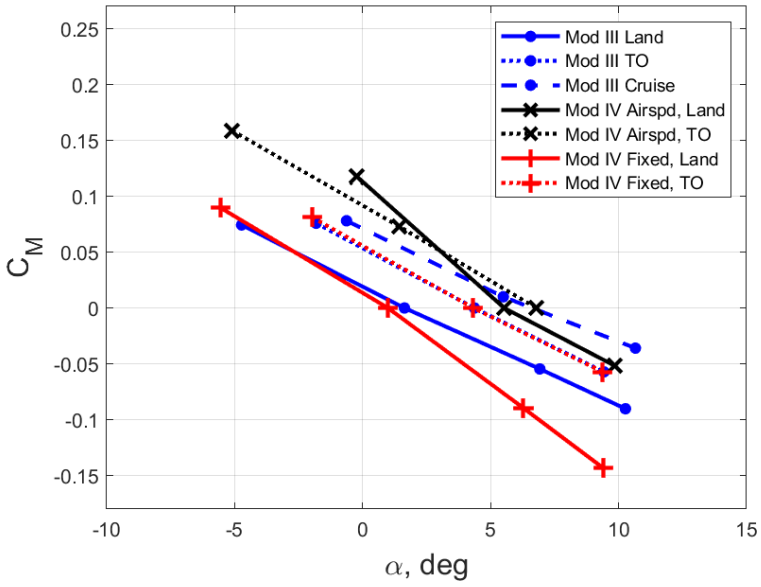

Fig.14 Pitching moment versus angle of attack for the Mod III aircraft and the Mod IV aircraft in the various aircraft configurations.

For subsonic aircraft, the longitudinal static stability also can be shown by a negative slope of the elevator position (δe) at trim versus the lift coefficient (C_L) curve [24]. Batch analysis studies of both the Mod III aircraft and the Mod IV aircraft were conducted at various airspeeds to determine the elevator positions at trim, as seen in Fig. 15. The elevator position versus lift coefficient curves are negative for both the Mod III aircraft and the Mod IV aircraft, indicating positive stability. Also seen in Fig. 15, both the Mod III aircraft and the Mod IV aircraft required trim elevator positions well within the control surface limits of -15 to 5 deg (positive deflection in trailing-edge down). As the C_L increases, the high-lift system for both airspeed and fixed modes appears to require less elevator deflection. The elevator trim position required also seems to be similar for both airspeed and fixed mode.

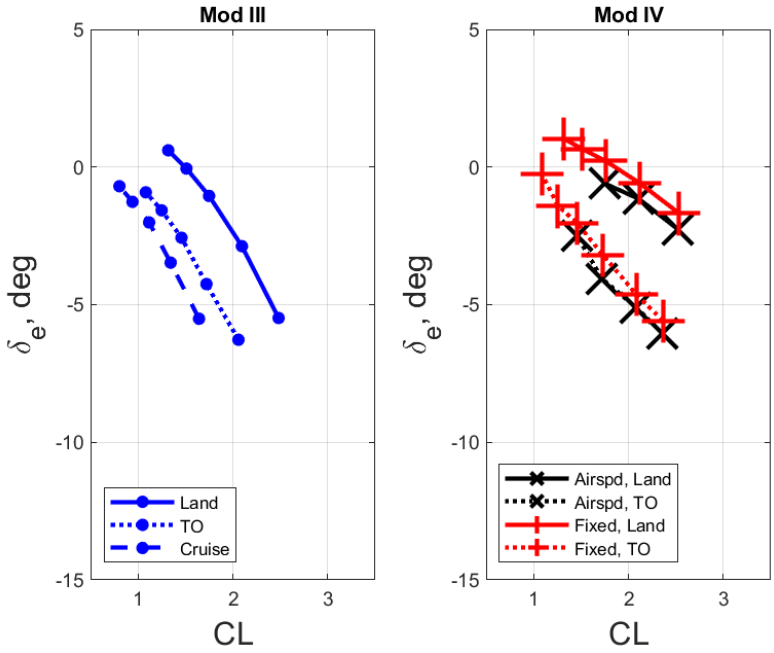

Fig. 15 Lift coefficient versus elevator trim position for the Mod III aircraft and the Mod IV aircraft in the various aircraft configurations.

Using FAR §23.177 to investigate the lateral stability in the pilot-in-the-loop simulator the X-57 project test pilots performed a lateral maneuver to demonstrate positive stability for both the Mod III aircraft and the Mod IV aircraft. The maneuver had the pilot, beginning from trim, establish a wings-level, steady sideslip, then release of both rudder and aileron controls. The pilots noted if the aircraft would recover to near-zero steady sideslip angle. The maneuver was conducted at various aircraft flap configurations, altitudes, and airspeeds to ensure stability throughout the flight envelope [23].

Figure 16 shows the piloted simulation data of the maneuver results for the- Mod III aircraft in the left panels and for the Mod IV aircraft on the right panels. After release of the yoke and rudder, the sideslip angle (β) in both the Mod III aircraft and the Mod IV aircraft, shown in Fig. 16, damped out to near 0 deg, thus exhibiting positive stability in the lateral direction.

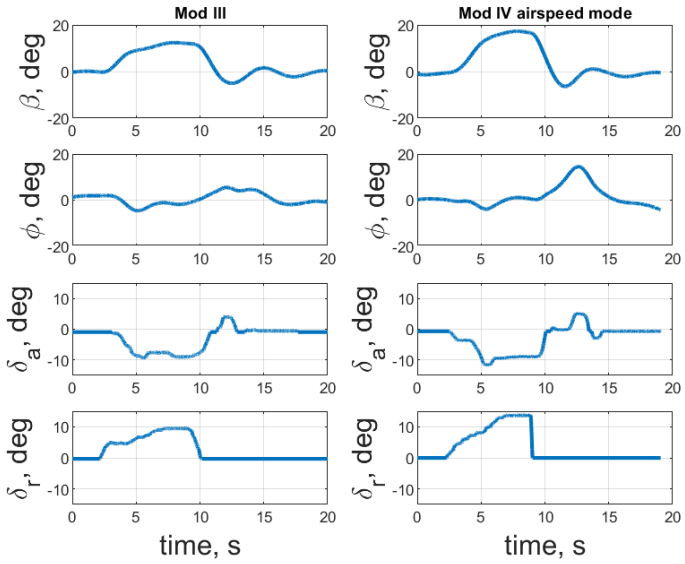

Fig. 16 Piloted simulator time histories for a steady wings-level sideslip maneuver for the Mod III aircraft and the Mod IV aircraft in takeoff configuration.

A lateral static stability analysis was conducted by examining the required rudder position (δr) and aileron position (δa) to maintain trim at various wings-level sideslip angles (β). A statically stable aircraft requires an opposite rudder input for an aileron input to maintain a given sideslip angle [24]; for example, a negative rudder input (trailing-edge left) requires a positive aileron input (right wing aileron down). Stability is demonstrated in Fig. 17 for both the Mod III aircraft and the Mod IV aircraft. The figure shows that for a given sideslip angle the aircraft requires an aileron command opposite to the rudder command.

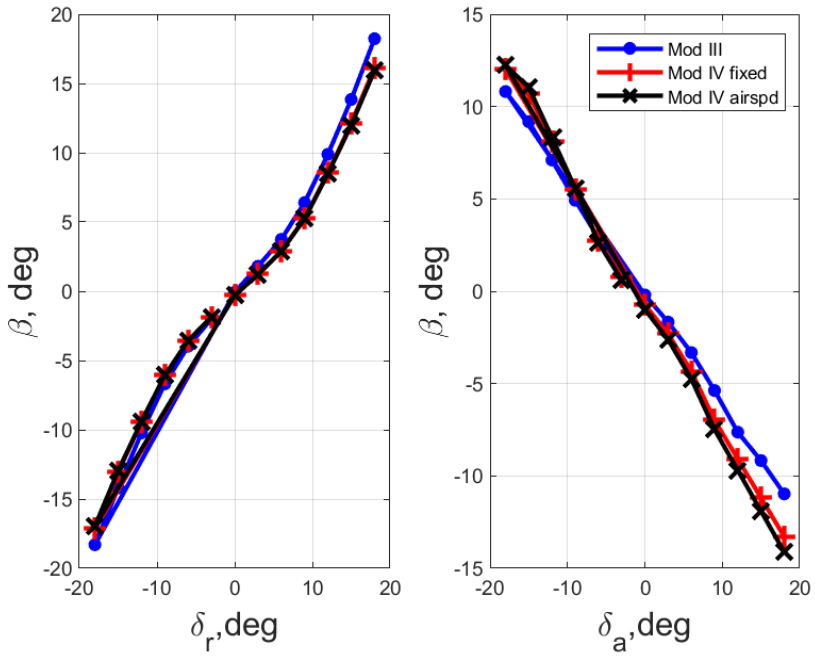

Fig. 17 In takeoff configuration: (left) simulation analysis of sideslip angle versus rudder position; (right) sideslip angle versus aileron position.

B. Linear Modal Analysis and Flying Qualities Predictions

To predict the dynamic stability throughout the flight envelopes of the Mod III aircraft and the Mod IV aircraft, the X-57 piloted simulator was used to obtain state-space models at various flight conditions and aircraft configurations. The predicted phugoid, short-period, roll, and Dutch roll mode requirements from the military standards handbook, MIL-STD-1797B [25], were used for the flying qualities of the assessments of the Mod III aircraft and the Mod IV aircraft. The Mod III and the Mod IV aircraft are small and light, and thus would be considered to be Class I per MIL-STD-1797B. A Level 1 assessment denotes having satisfactory flying qualities; a Level 2 assessment denotes having adequate flying qualities.

1. Phugoid Mode

The low-frequency longitudinal oscillations of the phugoid mode are easily controlled by the pilot; this mode is considered a nuisance mode. The eigenvalues for the phugoid mode for the Mod III aircraft and the Mod IV aircraft are shown in Fig. 18. Both the Mod III and the Mod IV aircraft are shown to be in the stable region of the polar plot in Fig. 18. For the Mod IV aircraft in airspeed mode the eigenvalues have a linear trend downward to the right on the polar plot except for the airspeed point of 96 KCAS, where there is a jump to the upward to the right. This condition is due to the aircraft being above the optimized airspeed region for the high-lift system, affecting the amount of lift and drag over the wing.

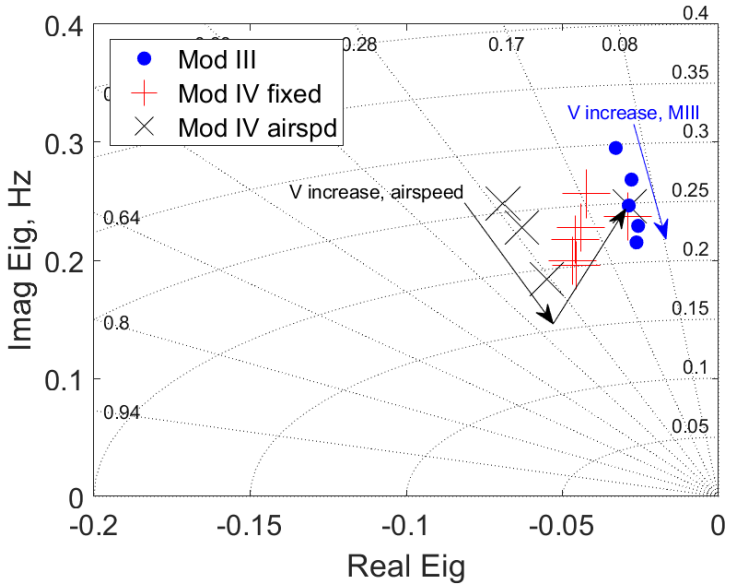

Fig. 18 Phugoid eigenvalues of the state space models for the Mod III aircraft and the Mod IV aircraft in takeoff configuration.

In addition, Fig. 19 shows the phugoid damping versus the calibrated airspeed for the Mod III aircraft and the Mod IV aircraft, plotted against the MIL-STD-1797B requirements. Level 1 flying qualities are shown for both throughout the flight envelope. At higher speeds of 96 KCAS, the airspeed phugoid of the Mod IV aircraft shows a significant drop in damping due to being outside the optimized lift scheduling for the high-lift system. As the speed increased for the fixed mode of the Mod IV aircraft, the damping seems to increase as airspeed increases until plateauing at approximately 100 KCAS.

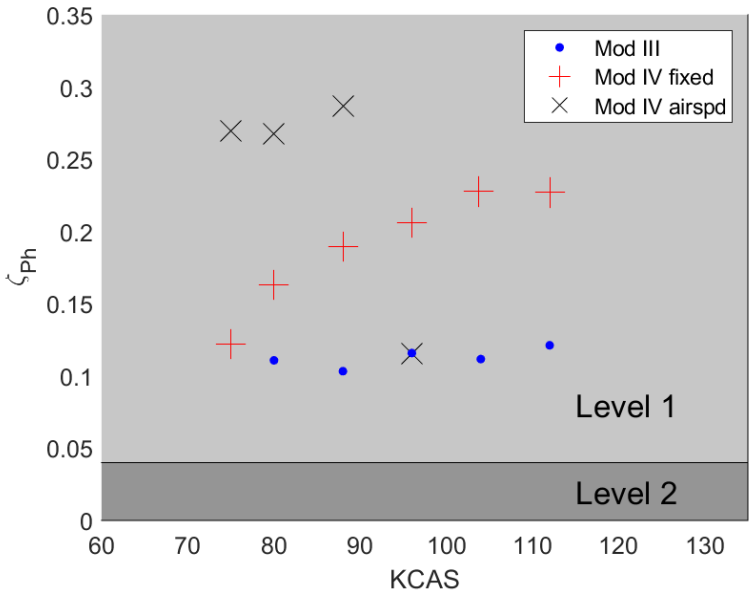

Fig. 19 Phugoid damping versus airspeed in takeoff configuration.

2. Short Period

The longitudinal short-period mode is characterized as higher frequency oscillations than the phugoid mode and can have a significant impact on the flying qualities of the aircraft. Figure 20 shows the state space model eigenvalues of the short-period mode for the Mod III aircraft and the Mod IV aircraft. The eigenvalues for both fall well within the stable region of the polar plot.

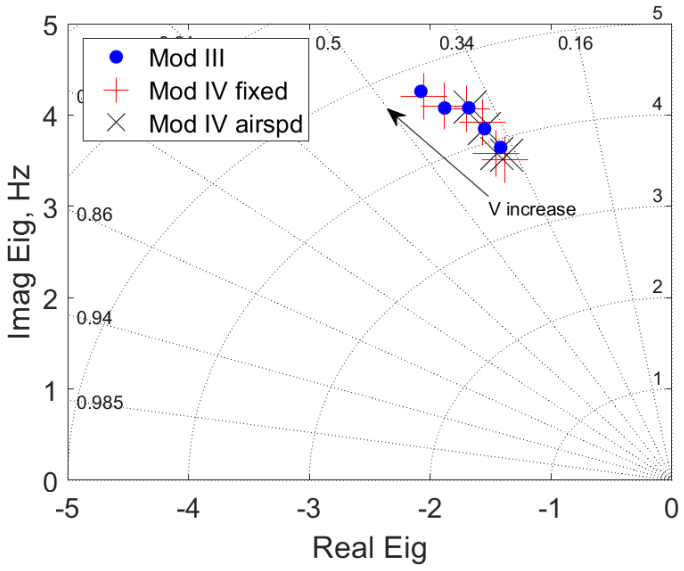

Fig. 20 Short-period eigenvalues of the state space models for the Mod III aircraft and the Mod IV aircraft in takeoff configuration.

The top panels of Fig. 21show the control anticipation parameter (CAP) versus the short-period damping along with the MIL-STD-1797 short-period requirements for both the Mod III aircraft and the Mod IV aircraft in the takeoff and landing phases of flight (Flight Phase Category C). The CAP, defined in Eq. (4), is the ratio of initial pitching acceleration to normal acceleration which represents the longitudinal sensitivity of the aircraft to a pitch command.

$$CAP \cong \frac{\omega_{sp}^2}{n/\alpha} \triangleq \frac{\omega_{sp}^2}{\frac{V_t}{g}\frac{1}{T}} \tag{4}$$

The short-period damping versus calibrated airspeed along with MIL-STD-1797B short-period requirements are shown in the bottom panels of Fig. 21. Looking at the top and bottom panels of Fig. 21, it is predicted that the Mod III aircraft and the Mod IV aircraft will have Level 1 flying qualities in airspeed mode, and that the Mod IV aircraft will have Level 1 flying qualities in fixed mode. The top panel of Fig. 21 shows an increasing CAP value for each aircraft as the short-period damping increases. The bottom panel of Fig 21 shows increasing short-period damping as the airspeed for each of the aircraft are increased.

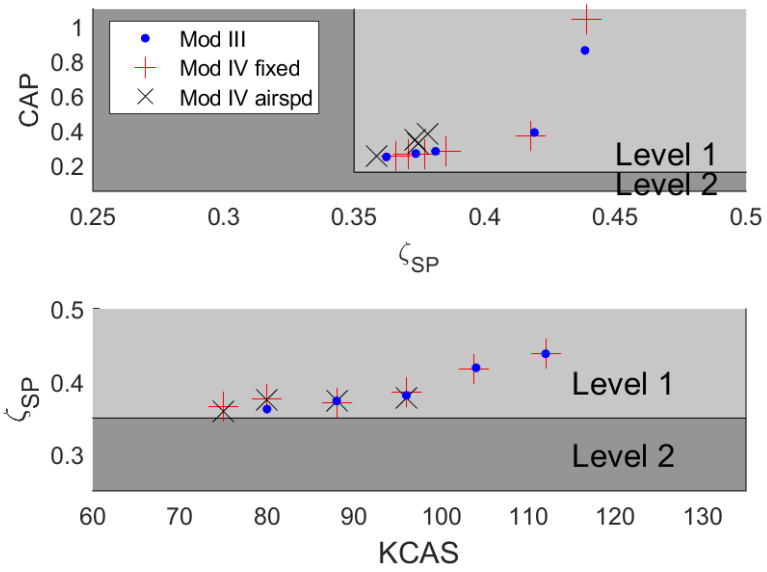

Fig. 21 In takeoff configuration: (top) the control anticipation parameter versus short-period damping; (bottom) short-period damping versus airspeed.

3. Roll Time Constant

The non-oscillatory, lateral roll mode is evaluated by examining the MIL-STD-1797 requirements in the takeoff and land phases of flight (Flight Phase Category C) for the roll mode time constant (τ_r) as a function of calibrated airspeed, shown in Fig. 22. The roll mode time constant indicates the quickness of the aircraft to develop a steady roll rate. At an airspeed of 73 KCAS it is predicted that in airspeed mode the Mod IV aircraft will have borderline Level 2 flying qualities. The rest of the flight envelope shows Level 1 flying qualities. As airspeed increases it is expected that the roll mode constant will decrease for each aircraft.

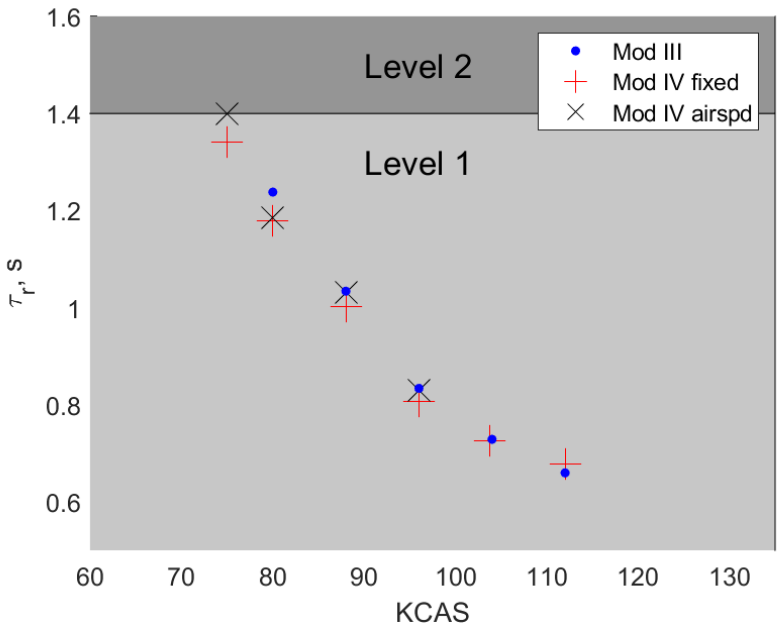

Fig 22. Roll mode time constant versus airspeed in takeoff configuration.

4. Dutch Roll

The oscillatory Dutch roll mode stability was investigated by examining the eigenvalues of the state space models on a polar plot, as seen in Fig. 23. The Dutch roll mode appears to be stable throughout the flight envelope for both the Mod III aircraft and Mod IV aircraft.

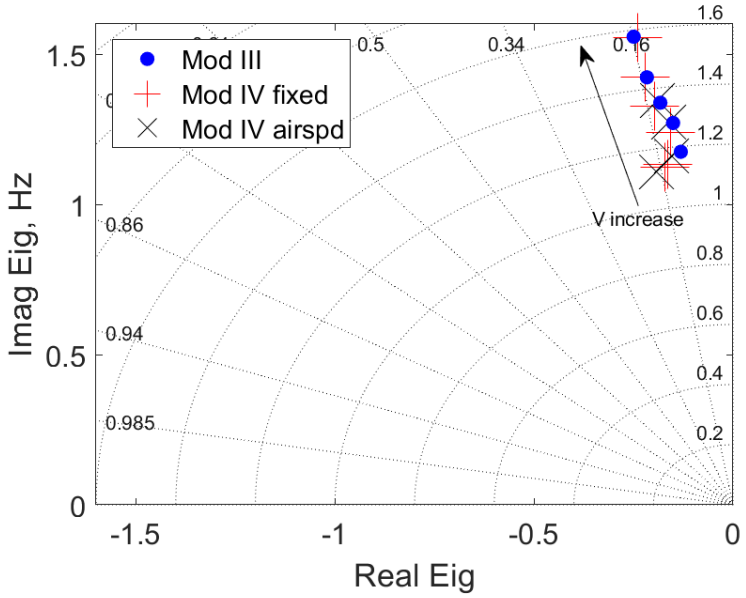

Fig. 23 Dutch roll mode eigenvalues of the state space models for the Mod III aircraft and the Mod IV aircraft in takeoff configuration.

Investigation of the Dutch roll mode examined the MIL-STD-1797 requirements in the takeoff and land phases of flight (Flight Phase Category C), as seen in Fig. 24. Figure 24 shows Dutch roll damping versus calibrated airspeed. It is predicted that both the Mod III aircraft and the Mod IV aircraft will have Level 1 flying qualities. As the airspeed

is increased from 73 KCAS, damping for both high-lift system modes decreases until approximately 90 KCAS, where the Dutch roll damping then increases. This effect shows that at low speeds, the high-lift system increases Dutch roll damping.

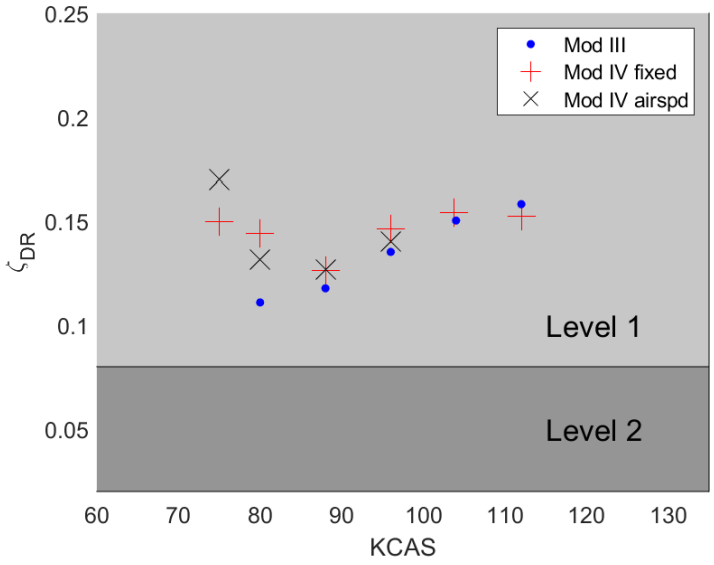

Fig. 24 Dutch roll mode damping versus airspeed in takeoff configuration.

V. Conclusion

A fixed-base pilot-in-the-loop nonlinear simulator has been developed for the Mod III and the Mod IV versions of the X-57 "Maxwell" aircraft. This simulator was used for flying quality prediction analysis, pilot training, failure analysis, and flight maneuver development.

The pilot simulator included integrated Mod III and Mod IV models of the propulsion, aerodynamics, landing gear, and mass properties. The propulsion model was developed to replicate the Mod III forces and moments of the wingtip motors, the unique Mod IV high-lift system, and the electrical system. The Mod III and the Mod IV aerodynamic models were developed using a large set of computational fluid dynamics cases to capture forces and moments from the effects of the wingtip propulsors, the high-lift system, and the cruise-optimized wing. The aerodynamic models also captured the predicted hinge moments and tail forces and moments. A fixed-base simulator cockpit was constructed to imitate the aircraft control surface inceptors, power effectors, a cockpit dashboard, electrical system switches, audio warnings, and out-the-window visuals.

Extensive Mod III and Mod IV stability and flying quality studies were conducted utilizing the piloted simulator. Guided by Federal Aviation Regulation Part 23, longitudinal and lateral maneuvers were performed by the X-57 project test pilots at various points in the flight envelope to provide stability predictions for both the Mod III and the Mod IV aircraft. The results of these studies showed that the aircraft will have static stability. Non-piloted simulation analyses of the lift coefficient versus elevator deflection, pitching moment versus angle of attack, and sideslip angle versus lateral control further showed additional static stability. The longitudinal and lateral eigenvalues from the linearization studies of both the Mod III and the Mod IV simulation models showed dynamic stability for both aircraft. The linearized simulation data were used also to evaluate the flying quality requirements of the MIL-STD-1797B for the phugoid, short-period, roll-time constant, and the Dutch roll modes. Based on the MIL-STD-1797B requirements, Mod III should have Level 1 flying qualities. Mod IV should have Level 1 flying qualities for the phugoid, short-period and Dutch roll modes but will have possible Level 2 for the roll mode time constant at lower airspeeds.

The fixed-base pilot-in-the-loop nonlinear simulator provided the X-57 project team with a means for pilot training, mission rehearsals, and evaluation and prediction of the flying qualities of both the Mod III and the Mod IV aircraft. With the cruise motors on the wingtip for the Mod III configuration, the piloted simulator became crucial to train the pilots for the highly dynamic failure scenario of a full-power single-power motor failure. The simulator also provided the pilots a tool to learn how to operate the high-lift system in flight. Throughout the development of the simulator, the X-57 project test pilots flew the simulator to provide feedback on both the aircraft handling qualities

and cockpit hardware human interaction. This feedback was invaluable to the project team in developing the aircraft models, cockpit design, and mission planning.

References

[1] Clarke, S., Redifer, M., Papathakis, K., Samuel, A., and Foster, T., "X-57 Power and Command System Design," *2017 IEEE Transportation Electrification Conference and Expo (ITEC)*, 2017, pp. 393-400. doi.org/10.1109/ITEC.2017.7993303

[2] Borer, N. K., et al., "Design and Performance of the NASA SCEPTOR Distributed Electric Propulsion Flight Demonstrator," AIAA Paper 2016-3920, June 2016. doi: 10.2514/6.2016-3920

[3] The Mathworks, Inc., MATLAB® and Simulink®, Software Package, Ver. 2016b, Natick, MA, https://mathworks.com [retrieved 21 May 2024].

[4] Castro, M., "AFRC Core Simulation Overview," NASA Document I.D. 20150007885, April 2015. https://ntrs.nasa.gov/search?q=AFRC%20Core%20Simulation%20Overview [retrieved 21 May 2024].

[5] Wallace, R., Reynolds, J., Frederick, M., McMinn, D., Cox, D., and Borer, N., "Development of the Mod II X-57 Piloted Simulator and Flying Qualities Predictions," AIAA Paper 2023-4034, June 2023. doi: 10.2514/6.2023-4034

[6] MT-Propeller, "MT-Propeller Operation and Installation Manual," ATA 61-01-18 (E-118), Revision 40, September 2014.

[7] Drela, M., Massachusetts Institute of Technology, Cambridge, Massachusetts, XROTOR, Software Package.

[8] Patterson, M. D., Borer, N. K., and German, B. J., "A Simple Method for High-Lift Propeller Conceptual Design," AIAA Paper 2016-0770, January 2016.

[9] doi: 10.2514/6.2016-0770
Borer, N. K., and Patterson, M. D., "X-57 High-Lift Propeller Control Schedule Development," AIAA Paper 2020-3091, June 2020. doi: 10.2514/6.2020-3091

[10] Litherland, B. L., Borer, N. K., and Zawodny, N. S., "X-57 "Maxwell" High-Lift Propeller Testing and Model Development," AIAA Paper 2021-3193, August 2021. doi: 10.2514/6.2021-3193

[11] Chin, J. C., Schnulo, S. L., Miller, T. B., Prokopius, K., and Gray, J., "Battery Performance Modeling on Maxwell X-57," AIAA Paper 2019-0784, January 2019. doi: 10.2514/6.2019-0784

[12] Wallace, R., Reynolds, J., and Borer, N., "Mitigation of High Lateral Asymmetry Rates Due to Loss of Cruise Motor on Mod III X-57, AIAA Paper (to be published for Aviation 2024, July 2024).

[13] Deere, K. A., Viken, J. K., Viken, S. A., Carter, M. B., Cox, D., Wiese M. R., and Farr, N., "Computational Component Build-up for the X-57 Distributed Electric Propulsion Aircraft," AIAA paper 2018-1275, January 2018. doi: 10.2514/6.2018-1275

[14] Yoo, S. Y., and Duensing, J. C., "Computational Analysis of the External Aerodynamics of the Unpowered X-57 Mod-III Aircraft," AIAA paper 2019-3698, June 2019. doi: 10.2514/6.2019-3698

[15] Yoo, S. Y., Duensing, J. C., Deere, K. A., Viken, J. K., and Frederick, M., "Computational Analysis on the Effects of High-lift Propellers and Wingtip Cruise Propellers on the X-57 Airplane," AIAA paper 2023-3382, June 2023. doi: 10.2514/6.2023-3382

[16] Frederick, M., Smith, M., Yoo, S., Wallace, R., Duensing, J., Houseman, J., Kiris, C., Deere, K., and Viken, J., "Development of the X-57 Aerodynamic Database," (to be published).

[17] Siemens Digital Industries Software, "Simcenter STAR-CCM+ CFD Software," Version 13.04.10. https://www.plm.automation.siemens.com/global/en/products/simcenter/STAR-CCM.html [retrieved 21 May 2024].

[18] Kiris, C. C., Housman, J. A., Barad, M. F., Brehm, C., Sozer, E., and Moini-Yeta, S., "Computational Framework for Launch, Ascent, and Vehicle Aerodynamics (LAVA)," *Aerospace Science and Technology,* Vol. 55, 2016, pp. 189-219. doi: 10.1016/j.ast.2016.05.008

[19] Frink, N. T., Pirzadeh, S. Z., Parikh, P. C., Pandya, M. J., and Bhat, M. K., "The NASA Tetrahedral Unstructured Software System (TetrUSS)," ICAS Paper No. 0241, August 2000.

[20] McDaniel, D. R., and Tuckey, T. R., "HPCMP CREATE™-AV Kestrel New and Emerging Capabilities," AIAA Paper 2020-1525, January 2020. doi: 10.2514/6.2020-1525

[21] Spalart, P. R., and Allmaras, S. R., "A One-Equation Turbulence Model for Aerodynamic Flows," AIAA Paper 92-0439, January 1992.

[22] Curry, A., Clarke, S., and Samuel, A., "X-57 Cockpit Display System Development and Features," AIAA Paper 2023-4035, June 2023. doi.org/10.2514/6.2023-4035

[23] Federal Aviation Administration (FAA), "Title 14–Aeronautics and Space," Code of Federal Regulations, Parts 1 to 59, 14 CFR Part 23, 2008.

[24] Yechout, T. R., Morris, S. L., Bossert, D. E., Hallgren, W. F., and Hall, J. K., *Introduction to Aircraft Flight Mechanics: Performance, Static Stability, Dynamic Stability, and Classical Feedback Control, and Space-State Foundations*, American Institute of Aeronautics and Astronautics, Inc., January 2014.
doi: 10.2514/5.9781624102547.0000.0000
https://www.govinfo.gov/content/pkg/CFR-2019-title14-vol1/pdf/CFR-2019-title14-vol1.pdf [retrieved 21 May 2024].

[25] Department of Defense Interface Standard "Flying Qualities of Piloted Aircraft," MIL-STD-1797, Rev. B, February 15, 2006, (Distribution Statement D).